



# Allosteric potentiation of a ligand-gated ion channel is mediated by access to a deep membrane-facing cavity

Stephanie A. Heusser<sup>a,b</sup>, Marie Lycksell<sup>a,b</sup>, Xueqing Wang<sup>a,b</sup>, Sarah E. McComas<sup>a,b</sup>, Rebecca J. Howard<sup>a,b</sup>, and Erik Lindahl<sup>a,b,c,1</sup>

<sup>a</sup>Department of Biochemistry and Biophysics, Stockholm University, 11419 Stockholm, Sweden; <sup>b</sup>Science for Life Laboratory, Stockholm University, 17165 Solna, Sweden; and <sup>c</sup>Swedish e-Science Research Center, KTH Royal Institute of Technology, 11428 Stockholm, Sweden

Edited by Michael L. Klein, Temple University, Philadelphia, PA, and approved September 11, 2018 (received for review June 12, 2018)

Theories of general anesthesia have shifted in focus from bulk lipid effects to specific interactions with membrane proteins. Target receptors include several subtypes of pentameric ligand-gated ion channels; however, structures of physiologically relevant proteins in this family have yet to define anesthetic binding at high resolution. Recent cocrystal structures of the bacterial protein GLIC provide snapshots of state-dependent binding sites for the common surgical agent propofol (PFL), offering a detailed model system for anesthetic modulation. Here, we combine molecular dynamics and oocyte electrophysiology to reveal differential motion and modulation upon modification of a transmembrane binding site within each GLIC subunit. WT channels exhibited net inhibition by PFL, and a contraction of the cavity away from the pore-lining M2 helix in the absence of drug. Conversely, in GLIC variants exhibiting net PFL potentiation, the cavity was persistently expanded and proximal to M2. Mutations designed to favor this deepened site enabled sensitivity even to subclinical concentrations of PFL, and a uniquely prolonged mode of potentiation evident up to ~30 min after washout. Dependence of these prolonged effects on exposure time implicated the membrane as a reservoir for a lipid-accessible binding site. However, at the highest measured concentrations, potentiation appeared to be masked by an acute inhibitory effect, consistent with the presence of a discrete, water-accessible site of inhibition. These results support a multisite model of transmembrane allosteric modulation, including a possible link between lipid- and receptor-based theories that could inform the development of new anesthetics.

ion channels | molecular dynamics | oocyte | general anesthetic | allostery

Despite the broad clinical relevance of general anesthetics to modern medicine, biophysical models of action remain incomplete and, in some cases, controversial. The early articulated Meyer–Overton theory highlighted the correlation between lipophilicity and potency in anesthetic agents, leading to models of nonspecific membrane disruption (1). Toward the end of the 20th century, however, focus shifted to membrane proteins, especially ion channels that mediate communication and excitability in the nervous system (2).

Among the most documented protein targets of general anesthetics are the pentameric ligand-gated ion channels (pLGICs), also known as Cys-loop receptors (3). This diverse family of membrane proteins includes both anion- and cation-conducting channels. General anesthetics decrease neuronal firing by potentiating many anionic pLGICs, including subtypes of glycine (4) and  $\gamma$ -aminobutyric acid type A (GABA<sub>A</sub>) receptors (5), and inhibiting several subtypes of cationic nicotinic acetylcholine (nACh) and serotonin type 3 (5-HT<sub>3</sub>) receptors (6). Further complexity is evident in  $\rho$ -subtype GABA<sub>A</sub> receptors, which are primarily inhibited by general anesthetics (7), and in the potentiation of certain nACh and 5-HT<sub>3</sub> receptors by small anesthetizing agents (8, 9). Given the structural similarity of many pLGICs, it is plausible that anesthetic binding sites are conserved; however, the molecular basis for their widely varying sensitivities remains unclear.

Until recently, crystallographic evidence for general anesthetic binding in pLGICs has been limited. Structures have been reported

for some eukaryotic family members, including GABA<sub>A</sub> (10, 11), glycine (12, 13), nACh (14), and 5-HT<sub>3</sub> receptors (15, 16). All structures consist of five subunits each containing a  $\beta$ -sheet extracellular domain and an  $\alpha$ -helical transmembrane domain, with the second transmembrane helices (M2) forming the ion pore (Fig. 1). However, no eukaryotic pLGIC structures have been determined in the presence of general anesthetics. Given the challenging nature of these targets, prokaryotic pLGICs are valuable model systems (17). In particular, the proton (H<sup>+</sup>)-gated *Gloeobacter violaceus* ligand-gated ion channel (GLIC) has now been crystallized in multiple apparent functional states (18–21) and with dozens of ligands, ions, or modulators.

In GLIC, the surgical agent propofol (PFL) was initially cocrystallized with the open wild-type (WT) channel, bound in a transmembrane cavity located within each subunit (22). In its WT form, GLIC is inhibited by most anesthetics, including PFL (23); therefore, this intrasubunit site was initially thought to represent a site of allosteric inhibition. It remained puzzling, however, why this presumed-inhibited complex remained in an apparent open state. In subsequent work, PFL was found to cocrystallize inside the closed channel pore (24), indicating an alternative mechanism of pore inhibition (Fig. 1).

In contrast to the initial association of the intrasubunit site with inhibition, multiple M2 helix variants confer net PFL potentiation rather than inhibition and convert the channel from crystallizing in an apparent closed to open conformation under identical conditions (24). A more complex profile resulted from

## Significance

Molecular mechanisms of general anesthetic modulation in pentameric ligand-gated ion channels remain controversial. Here we present molecular simulations and functional data that reveal correlations between dynamic differences in a membrane-accessible cavity and dramatic anesthetic effects, separate inhibitory and potentiating effects within the same electrophysiology recordings, and support a model for communication between the lipid bilayer and ion channel pore. In particular, enhanced electrostatic interactions in the membrane-accessible site were associated with a unique mode of anesthetic potentiation, persisting tens of minutes after washout. These results offer a bridge between lipid- and receptor-based theories of anesthesia, with the potential to inform both mechanistic understanding and drug development.

Author contributions: S.A.H., M.L., R.J.H., and E.L. designed research; S.A.H., M.L., and R.J.H. performed research; S.A.H., M.L., and R.J.H. analyzed data; S.A.H., M.L., R.J.H., and E.L. wrote the paper; X.W. and S.E.M. assisted experiments; and E.L. supervised experiments.

The authors declare no conflict of interest.

This article is a PNAS Direct Submission.

This open access article is distributed under [Creative Commons Attribution-NonCommercial-NoDerivatives License 4.0 \(CC BY-NC-ND\)](https://creativecommons.org/licenses/by-nc-nd/4.0/).

<sup>1</sup>To whom correspondence should be addressed. Email: erik.lindahl@scilifelab.se.

This article contains supporting information online at [www.pnas.org/lookup/suppl/doi:10.1073/pnas.1809650115/-DCSupplemental](http://www.pnas.org/lookup/suppl/doi:10.1073/pnas.1809650115/-DCSupplemental).

Published online October 1, 2018.

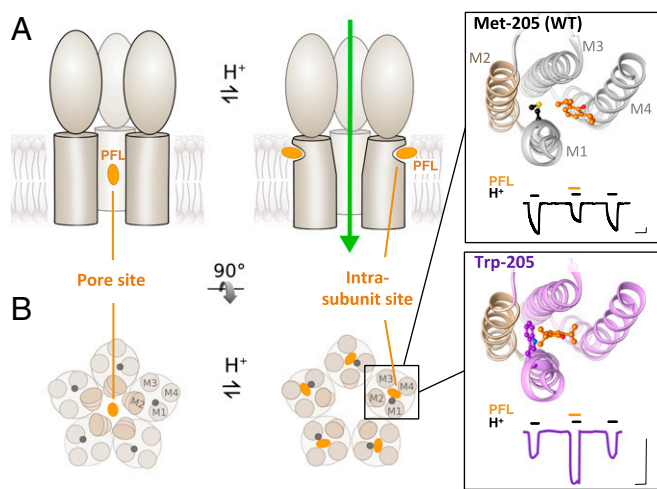


**Fig. 1.** Two types of general anesthetic sites in pGLICs. (A) Representative cartoons of GLIC, showing three of five subunits. Cocystal structures show PFL (orange) bound to a pore site in the closed channel (Left), or to an intrasubunit site in the open channel (Right). (B) Cross-sectional views of GLIC transmembrane domains (M1 to M4) as in A. (Inset) Zoom views of the intrasubunit cavity for WT (Top, PDB ID code 3P50) and Trp-205 crystal structures (Bottom, PDB ID code 5MVN), with PFL and position 205 in balls-and-sticks, and pore-lining helix M2 in tan. Electrophysiology traces show 30  $\mu$ M PFL inhibition of WT GLIC, and potentiation of Trp-205, respectively. (Scale bars, 1  $\mu$ A vs. 2 min.)

mutating the M1 Met-205 to Trp, which produced net potentiation by low to moderate concentrations of PFL, with inhibition restored at high concentrations (25). Crystallization of Trp-205 showed stabilization of PFL in the intrasubunit cavity (24). However, static structural data did not explain how dynamic conformational changes influence binding at the protein–lipid interface, nor how such subtle perturbations in structure dramatically alter sensitivity to a modulator with such low apparent affinity, and so few distinctive functional groups, as PFL.

In this work, we employed computational and electrophysiological methods to build a model for PFL modulation involving multiple, chemically distinct, sites in a pGLIC. Inhibitory effects were linked to a solvent-accessible site, while potentiating effects were related to the accessibility and dynamics of a membrane-accessible site. Enhanced electrostatic contacts in this latter site were associated with a considerably prolonged mode of potentiation, not previously observed to our knowledge, possibly bridging protein hypotheses of general anesthetic action with longstanding lipid-based theories.

## Results

**M1-205 Mutations Increase Membrane Access to M2 and Enable PFL Potentiation.** To visualize conformational changes underlying differential modulation in GLIC, we performed triplicate 1- $\mu$ s molecular dynamics simulations based on cocystal structures of M1-205 variants exhibiting inhibition [WT/Met-205, Protein Data Bank (PDB) ID code 3P50] or potentiation (Trp-205, PDB ID code 5MVN) by moderate concentrations of PFL (25). For a majority of simulation frames, PFL remained in the crystallographic binding site (SI Appendix, Fig. S1 A and B). We also performed equivalent simulations of Met and Trp variants with PFL removed, enabling us to compare binding site dynamics in holo and apo states. In all simulations, protein C $\alpha$  root-mean-square deviations (RMSDs) stabilized below 2.1  $\text{Å}$  within 200 ns, and the pore remained hydrated (SI Appendix, Figs. S2 A and B and S3 A–C). In both holo and apo simulations, lipid tails entered the vestibule of the binding cavity, making frequent contacts with cavity-lining residues and, in holo simulations, PFL itself (SI Appendix, Fig. S4A).

In WT (Met-205) holo simulations (Fig. 2 A and B, black), the intrasubunit cavity had a mean volume somewhat greater than in comparable cocystal structures, or the molecular volume of PFL ( $\sim 300 \text{Å}^3$ ). Upon PFL removal, the cavity volume decreased by at least 75%, to volumes well below that of PFL (Fig. 2 A and B, black). The reduction in volume was also associated with decreased penetration toward the channel pore, as measured by a doubling in distance from the cavity perimeter to the nearest pore-lining M2 helix residue (Val-242) in apo vs. holo simulations (Fig. 2C, black). In contrast, intrasubunit cavities were less

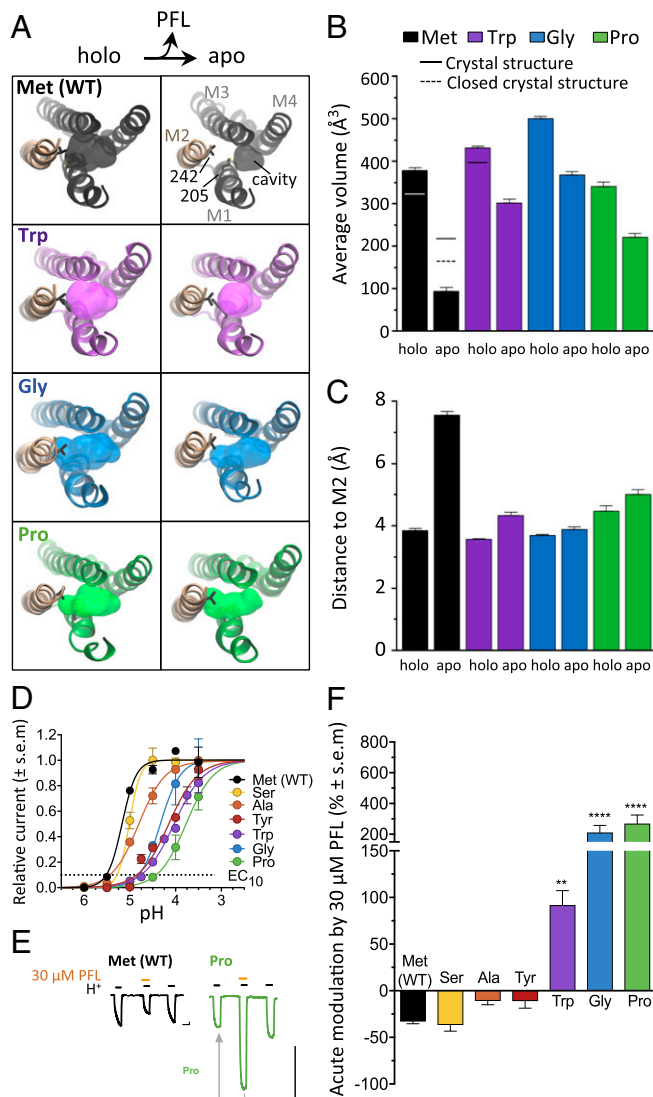


**Fig. 2.** M1-205 mutations increase membrane access to M2 and enable PFL potentiation. (A) Top views as in Fig. 1B of representative frames from holo (Left) and apo (Right) simulations for Met (WT) and M1-205 variants Trp, Gly, and Pro. Surfaces show the PFL binding cavity, with residues M1-205 and M2-242 as sticks. (B) Mean intrasubunit cavity volumes for simulations (columns) and previous X-ray structures (lines). (C) Mean shortest distance between the pocket perimeter and M2 Val-242. In B and C, columns represent mean values  $\pm$  block error estimates. (D) Normalized concentration–response curves for H<sup>+</sup> activation of M1-205 variants (EC<sub>10</sub> as dotted line). (E) Sample traces for WT (black) and Pro-205 (green) showing EC<sub>10</sub> activation pretreatment, then cotreatment with 30  $\mu$ M PFL, then posttreatment. Arrow indicates comparison in F. (Scale bars, 1  $\mu$ A vs. 2 min.) (F) Acute modulation of GLIC M1-205 variants by 30  $\mu$ M PFL, calculated as percent change in cotreatment vs. pretreatment currents. Significance is relative to WT, one-way analysis of variance,  $n = 4$  to 8 (\*\* $P < 0.01$ ; \*\*\*\* $P < 0.0001$ ).

affected by PFL removal in Trp-205 (Fig. 2A, purple). Cavities in Trp-205 apo simulations decreased <30% vs. holo simulations, remaining around the volume of PFL (Fig. 2B, purple), and retaining proximity to M2 (Fig. 2C, purple). Computational docking demonstrated a parallel pattern of PFL accessibility in experimental GLIC structures, with more-favorable intrasubunit binding poses in the Trp variant relative to WT (SI Appendix, Fig. S5).

Given the apparent influence of position 205 on intrasubunit cavity dynamics, we asked whether substitutions other than Trp also alter PFL sensitivity. In two-electrode voltage clamp electrophysiology experiments in *Xenopus* oocytes, substituting Met-205 with Ser, Ala, or Tyr produced channels with intermediate agonist sensitivity between WT (Met) and Trp variants (Fig. 2D), and moderate net inhibition by 30  $\mu$ M PFL, similar to WT (Fig. 2E and F). Substitutions to Gly or Pro—residues associated with helix disruption (26)—produced potent potentiation by 30  $\mu$ M PFL, more than twice as strong as with Trp (Fig. 2E and F). Cotreatment with 300  $\mu$ M PFL in the Gly-205 or Pro-205 variants produced less potentiation than 30  $\mu$ M or 100  $\mu$ M, similar to the bimodal effects seen in the Trp variant, and resulted in net inhibition in most of the variants tested (SI Appendix, Fig. S6B and C). Pro-205 exhibited the greatest sensitivity to potentiation, enhanced by as little as 1  $\mu$ M PFL, and retained modest potentiation even by 300  $\mu$ M PFL (SI Appendix, Fig. S6A and C).

We returned to molecular dynamics to visualize the effects on PFL sensitivity of Gly and Pro substitutions. In triplicate 1- $\mu$ s simulations of Gly-205 and Pro-205 systems in the presence and absence of PFL, protein C $\alpha$  RMSDs again converged within 200 ns, and pores remained largely hydrated (SI Appendix, Figs. S2C and D and S3A, D, and E). As in the Trp variant, the intrasubunit cavity of Gly and Pro variants exhibited little contraction upon PFL removal (Fig. 2A, blue and green), dropping less than 50% in cavity volume (Fig. 2B, blue and green) and remaining within 4.5  $\text{Å}$  of the nearest contact in M2 (Fig. 2C, blue and green).

### Helix-Disrupting Residues at M1-205 Enable Persistent PFL Potentiation.

In addition to altering dynamics of cavity volume and penetration, the Gly and Pro substitutions disrupted native backbone hydrogen bonding in the upper portion of M1 (Fig. 3A, black). In many frames of the Gly- and Pro-variant simulations, the Ile-202 backbone O atom reoriented into the intrasubunit cavity, creating a hydrogen bond with the hydroxyl group of PFL (Fig. 3A, green). Indeed, in >25% of simulation frames for both Gly and Pro variants, we found the PFL hydroxyl group within 3.5  $\text{Å}$  of the Ile-202 carbonyl, while, in WT (Met) and Trp-variant simulations, such proximity was only observed in <8% of frames (Fig. 3B).

In parallel with this alternative mode of intermolecular electrostatic interaction, Gly and Pro substitutions at M1-205 were associated in electrophysiology experiments not only with potent acute potentiation (Fig. 2F) but also with dramatically prolonged effects of high PFL exposure, not previously documented to our knowledge. Specifically, exposure to 100  $\mu$ M PFL enhanced channel activation well after 5 min washout (Fig. 3C, Inset, green, and SI Appendix, Fig. S7A), producing a posttreatment peak >4 times larger than the pretreatment peak for both Gly and Pro variants (Fig. 3C, blue and green). Upon exposure to 300  $\mu$ M PFL, persistent effects on the posttreatment peak were even more pronounced (SI Appendix, Fig. S6E). Prolonged potentiation decreased over time independent of channel activation (Fig. 3C, Inset, green, and SI Appendix, Fig. S7A). No such pronounced posttreatment effects were observed for inhibition of Met, Ser, Ala, or Tyr variants, for potentiation of the Trp variant, nor at lower PFL concentrations (Fig. 3C and SI Appendix, Fig. S6D and E).

We next asked whether persistent potentiation depended on channel activity, or simply on the extent of PFL exposure. Following an initial pretreatment activation, we exposed Pro-205 channels to 100  $\mu$ M PFL for various durations without activating the channels, washed out the PFL for 5 min, then activated channels again (Fig. 3D). In the absence of activation, PFL had no direct effect on channel activity; however, this “silent” exposure to PFL for 0.5, 1, 3, or 6 min potentiated posttreatment currents roughly 2-, 3-, 6, or 6.7-fold, respectively (Fig. 3D and E).

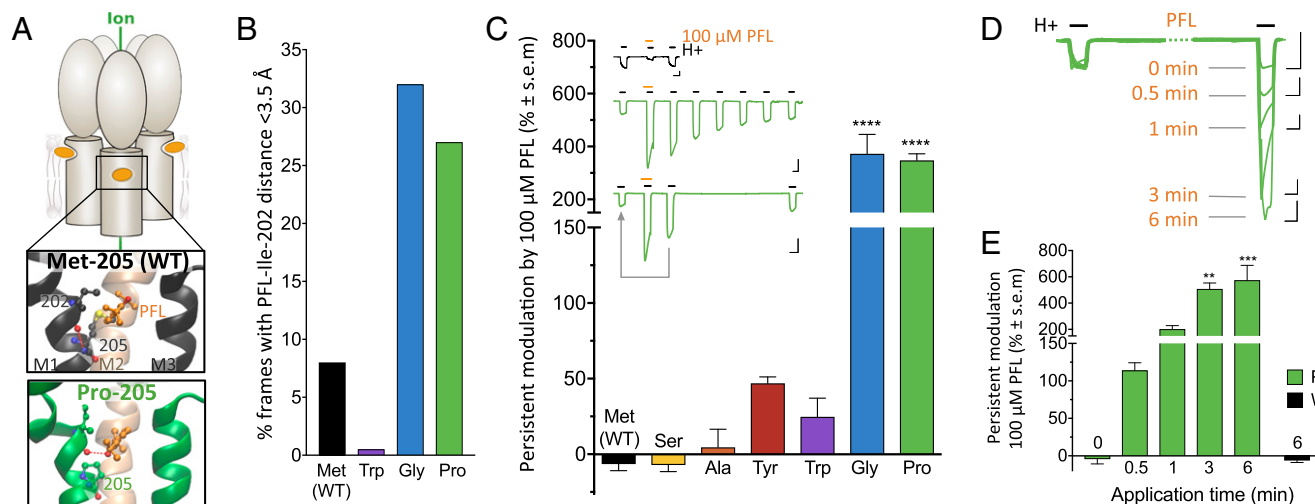


**Fig. 3.** Helix-disrupting residues at M1-205 enable persistent PFL potentiation. (A) Cartoon of GLIC, with zoom views of helices M1 to M3 showing PFL (orange) and neighboring residues, colored by heteroatom, for WT (black) and Pro-205 (green). Dashes indicate representative hydrogen bonds between carbonyl O of Ile-202 and either the backbone N of Leu-206 (WT) or hydroxyl O of PFL (Pro-205). (B) Fraction of simulation frames in which the PFL hydroxyl is <3.5  $\text{Å}$  from the Ile-202 carbonyl. (C) Persistent modulation of M1-205 variants by 100  $\mu$ M PFL, calculated as percent change in posttreatment vs. pretreatment currents. (Inset) Sample traces as in Fig. 2E showing 100  $\mu$ M PFL cotreatment. For Pro-variant traces,  $\geq$ 35-min posttreatment activations are also shown. Arrow indicates comparison in graph. (Scale bars, 2  $\mu$ A vs. 2 min.) (D) Time dependence of persistent PFL effects in Pro-205. Overlaid sample traces show activation pretreatment, then posttreatment with exposure to 100  $\mu$ M PFL for varying amounts of time in between. (Scale bars, 1  $\mu$ A vs. 2 min.) (E) Time dependence from the protocol in D, with control 6-min treatment of WT, calculated as percent change in posttreatment vs. pretreatment currents. In C and E, significance is relative to WT or 0-min exposure, respectively; one-way analysis of variance,  $n = 4$  to 11 (\*\* $P < 0.01$ ; \*\*\* $P < 0.001$ ; \*\*\*\* $P < 0.0001$ ).

Similar results were obtained for silent PFL treatment of Gly-205 (*SI Appendix, Fig. S7 B and C*).

To determine whether these persistent effects are specific to PFL, we tested the two alternative anesthetizing agents bromoform and ethanol, which have been shown to bind the same cavity as PFL (27). Cotreatment with either bromoform (1 mM) or ethanol (600 mM) potentiated Met, Trp, and Gly variants, but did not produce posttreatment effects greater than  $\pm 50\%$  after a 5 min-washout (*SI Appendix, Fig. S8*).

**Inhibition Unmasked at High PFL Concentrations.** In addition to acute and persistent potentiation of helix-perturbed GLIC variants, we observed an additional, opposing mode of inhibition at 300  $\mu\text{M}$  PFL, the highest concentration tolerated by our system. During cotreatment with 300  $\mu\text{M}$  PFL, currents were smaller than upon activation after a 5-min subsequent washout (Fig. 4A). To test whether this submaximal cotreatment effect resulted from delayed potentiation, or from a conflicting mode of acute inhibition, we extended the recording protocol: Currents increased roughly twofold upon cotreatment with 300  $\mu\text{M}$  PFL, but increased fourfold posttreatment. Subsequent 300- $\mu\text{M}$  cotreatment in the same oocyte reproduced the initial, twofold current, with fourfold currents restored posttreatment (Fig. 4A, *Bottom*). Despite dramatic differences in acute potentiation (cotreatment vs. pretreatment currents; Fig. 2F), all variants exhibited inhibition of 300- $\mu\text{M}$  cotreatment vs. posttreatment currents, in a relatively narrow range of 45% to 80% (Fig. 4). Thus, cotreatment with 300  $\mu\text{M}$  PFL appeared to reveal an acute, reversible mode of inhibition that could transiently mask potentiation, and was relatively conserved. Computational docking revealed a pattern consistent with pore inhibition, where PFL adopted poses proximal to Ser-230 and Ala-237. Pore poses—particularly near Ala-237—were favored in closed-state GLIC, but less so relative to the intrasubunit site in open-state structures (*SI Appendix, Fig. S5*).

## Discussion

Computational and electrophysiology data in this work shed light on controversies in mechanistic studies of general anesthesia. Optimization of an intrasubunit site for PFL binding enabled separation of potentiating and inhibitory modes of modulation within the same recording, which offers a conceptual bridge between historic lipid-based and recent protein-based mechanisms of action. Our resulting model highlights the value of dynamic, high-resolution structural information in elucidating general anesthetic modulation, and likely in providing templates for rational drug design.

Binding of PFL to the membrane-accessible intrasubunit cavity in WT GLIC has previously been associated with inhibitory effects (22). In this work, however, inhibition was linked to binding to a primarily solvent-accessible site, as inhibition was

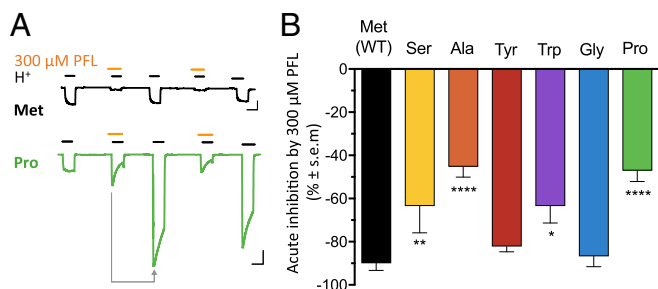
stronger during PFL perfusion but relieved when PFL was washed off, unmasking strong potentiating allosteric effects (Fig. 4A). Additionally, mutations of the intrasubunit cavity-lining Met-205 had strong effects on potentiation (Fig. 2F) but less so on inhibition (Fig. 4B), indicating a topologically distinct site for inhibition. Based on past structural studies of PFL in GLIC (24) and *Erwinia chrysanthemi* ligand-gated ion channel (28), as well as labeling studies in nACh (29) and GABA<sub>A</sub> receptors (30), we expect this inhibition to result from binding to the pore. Computational docking provided further support for pore-mediated inhibition, particularly via a previously reported site near Ala-237 (24, 31), indicating preferential binding to, and allosteric stabilization of, the closed vs. open states (*SI Appendix, Fig. S5*). We cannot, however, rule out contributions of other inhibitory mechanisms.

In contrast, our results offer evidence for a role of the intrasubunit cavity in potentiation. Selected Met-205 mutations produced channels that were strongly potentiated by PFL and remained potentiated (but not inhibited) even when PFL was removed from solution, while residual PFL likely remained in the membrane (Fig. 3 C–E). These potentiated channels presented larger cavities that reached far toward the pore-lining helix M2 (Fig. 2 A–C), facilitating open-state hydrophobic interactions between M2 (Val-242) and PFL as well as other cavity-defining residues not expected in closed channels, where M2 retreats away from the intrasubunit site toward the pore (19). Thus, deep intrasubunit PFL binding stabilized contacts that favor the open state (24)—a model that agrees with classical allosteric theories in which potentiation arises from increased affinity to the activated state and consequent stabilization thereof (32). PFL potentiation via the intrasubunit site has been further supported by molecular dynamics (31), thiosulfonate labeling (33), and structural work (24). Thus, static structures parallel dynamic data in this work to implicate the intrasubunit cavity as a general site of GLIC potentiation. Previous studies in eukaryotic channels, particularly nACh receptors (34–36), validate the concept of positive anesthetic modulation mediated by an intrasubunit site.

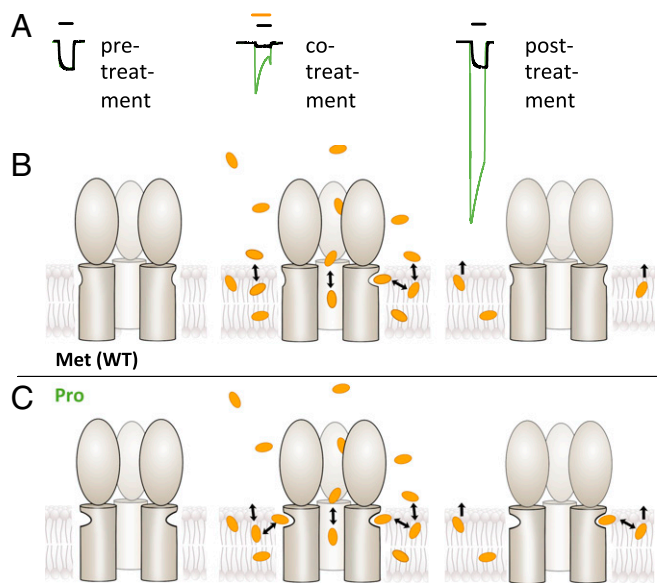
Notably, the three M1-205 variants (Trp, Gly, and Pro) with expanded forms of the open-state intrasubunit cavity also exhibited decreased H<sup>+</sup> sensitivity, in accordance with a critical role for the extracellular-facing portion of M1 in gating and modulation (37). Previous studies in GLIC (38, 39), nACh (40, 41), and 5-HT<sub>3</sub> receptors (42, 43) have shown that disruption of backbone N hydrogen bonding at Pro-204—the most conserved transmembrane residue among all pLGICs (44)—is not only permissive, but necessary for channel gating. It is plausible that bulky or helix-disrupting residues at adjacent position 205 could account for an increased barrier to relieving the M1 kink, decreasing agonist sensitivity but increasing accessibility of M2 from the membrane.

Fig. 5 illustrates a proposed model for high-concentration PFL effects in the presence (Fig. 5B) and absence (Fig. 5C) of selected M1-205 substitutions. In this model, GLIC variants containing Trp, Gly, or Pro at position 205 contain a relatively stable deep intrasubunit cavity facilitating communication between the membrane and the pore-lining M2 helix (Fig. 5C, *Left*). Accordingly, PFL has a high capacity to bind and allosterically stabilize the open state (Fig. 5C, *Center*). Lipophilic PFL molecules readily partition into the membrane, where they diffuse into membrane-accessible protein sites. However, diffusion back into the perfusion medium is expected to be considerably slower; thus, even upon washout, residual PFL in the membrane remains in equilibrium with highly sensitive intrasubunit sites in the Gly-205 and Pro-205 variants, producing persistent potentiation (Fig. 5C, *Right*). In the simpler case of lower ( $\sim 30 \mu\text{M}$ ) concentrations, PFL produces only acute inhibition and potentiation in WT or M1-variant GLIC, respectively (*SI Appendix, Fig. S9*).

This work builds on past proposed mechanisms of bimodal PFL effects (24, 31), providing both an approach to distinguish inhibition and potentiation in a single functional recording and



**Fig. 4.** Inhibition unmasked at high PFL concentrations. (A) Sample traces as in Fig. 2E with 300  $\mu\text{M}$  PFL cotreatment, repeated. Arrow indicates comparison in graph B. (Scale bars, 2  $\mu\text{A}$  vs. 2 min.) (B) Acute inhibition of GLIC M1-205 variants by 300  $\mu\text{M}$  PFL, calculated as percent difference between cotreatment and posttreatment currents. Significance is relative to WT, one-way analysis of variance,  $n = 4$  to 10 ( $*P < 0.05$ ;  $**P < 0.01$ ;  $****P < 0.0001$ ).



**Fig. 5.** Model for differential PFL modulation in intrasubunit variants of a model pLGIC. (A) Overlaid sample traces for GLIC WT (black) and Pro-205 (green) as in Fig. 4. (B) In the absence of PFL (Left), intrasubunit cavities in WT GLIC (Met-205) are largely contracted. These cavities must expand to bind PFL (Center), resulting in relatively little current enhancement, while the dominant effect is inhibition via pore binding. Washout (Right) removes PFL from the aqueous-accessible pore; intrasubunit sites contract upon unbinding, lowering their affinity and rendering them insensitive to residual PFL in the membrane. (C) In GLIC Pro-205 and related variants, intrasubunit cavities are relatively deep even in the absence of PFL (Left). Upon cotreatment (Center), PFL can bind with little cavity expansion, producing potentiation only partly compensated by inhibitory binding in the pore. After washout (Right), high-affinity intrasubunit cavities may still bind residual PFL in the membrane, producing potentiation unopposed by inhibition. In B and C, three subunits of GLIC are represented as in Fig. 1A.

stably-open channel simulations that can account for enhanced potentiation in selected variants. We therefore believe this model (Fig. 5) is the most parsimonious fit to past and present structural, computational, and functional data, although alternatives are possible. We also considered whether PFL might unbind slowly from these receptor variants, producing persistent effects many minutes after removal from the buffer. However, on the timescale of our simulations, PFL dissociation events were similar in all variants (*SI Appendix, Fig. S1*), indicating that substitutions more likely affected the equilibrium of bound/unbound receptors. Transient PFL exposure might induce an alternative, long-lived, highly agonist-sensitive conformation in Gly-205 and Pro-205 receptors, resulting in enhanced  $H^+$  activation even after PFL unbinding. However, we saw no evidence for transition to an alternative functional state, even at the level of protein RMSD (*SI Appendix, Fig. S2*). Furthermore, such a mechanism would not be expected to increase with PFL exposure time, as observed here (Fig. 3D and E and *SI Appendix, Fig. S7 B and C*). Moreover, treatment with considerably higher concentrations of bromoform or ethanol—despite conferring acute potentiation, and binding to the same intrasubunit site (20, 45)—produced no long-term effects (*SI Appendix, Fig. S8*). A key distinction between these agents and PFL is their lipophilicity [ $\log P$ : bromoform, 2.5 (46); ethanol,  $-0.31$ ; and PFL, 3.79 (47)], consistent with a mechanism based on persistence in the membrane. Closed-pore structures of GLIC revealed no intrasubunit density for PFL (24), and only weak signal for the smaller agent bromoform (48). It is plausible that an alternative agent could preferentially bind to the constricted intrasubunit site in the resting state, or a related region in a desensitized or alternative nonconducting state, producing channel inhibition. Differential

effects from asymmetric PFL unbinding can also not be excluded (49), but were not observed on the timescales of our simulations, nor in X-ray structures (24). Analysis of the data in this work strongly supports preferential PFL access in the open state, producing potentiation.

In the Gly-205 and Pro-205 variants, persistent sensitivity to PFL potentiation could be linked to increased hydrogen bonding between PFL molecules and the protein backbone observed in our simulations. Notably, Gly and Pro are never seen at the equivalent position in native pLGICs (*SI Appendix, Fig. S10*), and, to our knowledge, no native pLGICs have been shown to exhibit the persistent PFL effects documented here. It is plausible that helix-disrupting residues at position 205 have been precluded by evolution, possibly to avoid hypersensitivity to small alcohols, lipid metabolites, or other endogenous agents analogous to PFL.

In all high-resolution open-state GLIC structures, but not in nonconducting structures, a lipid occupies the membrane-facing vestibule of the intrasubunit cavity (18, 19). Similar lipids contact intrasubunit-bound PFL in our holo-state simulations as well as in WT and mutant X-ray structures (22, 24). Thus, intrasubunit PFL may mediate or mimic positive endogenous modulation by membrane lipids. It is particularly suggestive that the intrasubunit cavity directly contacts both the membrane and the pore-lining M2 helix, specifically Val-242, which moves  $>5 \text{ \AA}$  between closed and open states. The intrasubunit cavity—at least in its expanded state—could serve as a conduit for direct communication between the membrane and ion conduction pathway.

As demonstrated by previous functional and biochemical studies, the primary physiological targets of PFL, GABA<sub>A</sub> receptors, add complexity to the landscape of pLGIC modulation in the form of an alternative interaction site at the transmembrane subunit interface (50). However, in WT GLIC—and evidently all of the intrasubunit variants explored in this work—intersubunit PFL binding is precluded by bulky side chains at the subunit interface, particularly Phe-238 and Asn-239 (20, 24), enabling the isolation of intrasubunit from intersubunit effects. Despite the topological distinction of intrasubunit and intersubunit PFL sites that predominate in GLIC and GABA<sub>A</sub> receptors, respectively, the effects of these sites may be closely related. Earlier efforts at computational drug screening based on the GLIC intrasubunit site yielded hit compounds that appeared to potentiate GABA<sub>A</sub> receptors via the intersubunit site (25), suggesting that the PFL pharmacophore is generalizable to neighboring transmembrane sites, or that access to one site facilitates modulation via the other. Indeed, analysis of the first GLIC–PFL crystal structure described the intrasubunit site as contiguous with the (smaller) intersubunit site, by way of a constricted “linking tunnel.” If a similar pathway is employed in GABA<sub>A</sub> receptors, intrasubunit interactions could contribute to a PFL conduit from the membrane to more deeply buried labeling targets in the intersubunit cavity. Mechanisms involving these two sites might be related, as M1 interactions appear important for intersubunit PFL binding in GABA<sub>A</sub>-Rs (51), and potentiation of homologous channels by ivermectin has been similarly associated with cavity expansion (13, 52). An important extension will be to validate this model by applying similar computational approaches to pLGIC variants with PFL-accessible intersubunit binding sites.

This work affirms the capacity of the intrasubunit transmembrane site to mediate pLGIC potentiation, documents an influential role of the M1 helix in modulation as well as gating, reports a unique mode of prolonged current enhancement in helix-disrupted variants, and implicates a mode of communication between the membrane and the channel pore. The lipophilic nature of PFL appears unexpectedly valuable in dissecting its opposing effects at discrete sites and providing a conceptual link to lipid-oriented theories of anesthesia (1). Based on our results, it is likely that future drug development of allosteric modulators will depend on the integration of dynamic simulations, atomic resolution structures, and electrophysiological recordings to

identify state-specific binding sites and structural consequences of their interactions.

## Materials and Methods

**Molecular Dynamics Simulations, Docking, and Analysis.** As starting models for molecular dynamics, we used PFL cocrystal structures for WT (Met-205, PDB ID code 3P50; ref. 22) and Trp-205 (PDB ID code 5MVN; ref. 24) GLIC variants. Apo structures were generated by deleting PFL. The Gly-205 variant was built on the equilibrated holo Trp-205 template and used as a template for Pro-205. Each protein was embedded in a 1-palmitoyl 2-oleoyl phosphatidylcholine lipid bilayer, solvated with 0.1 M NaCl, and protonated to approximate activating conditions (22). For each model, equilibration and three 1- $\mu$ s simulations were run with Gromacs 2016.1 (53) and analysis of the trajectories performed with VMD (54) and MDpocket (55). Computational docking was

performed using AutoDock Vina (56). For more detailed information, see *SI Appendix, SI Materials and Methods*.

**Oocyte Electrophysiology.** Plasmid preparation, oocyte expression, and two-electrode voltage clamp recordings were performed as previously described (24). Each anesthetic modulation protocol was carried out on a previously untreated oocyte, using 10% maximal ( $EC_{10}$ ) activating conditions calibrated for the appropriate mutant. For detailed information, see *SI Appendix, SI Materials and Methods*.

**ACKNOWLEDGMENTS.** We thank the Knut and Alice Wallenberg Foundation, the Swedish Research Council, the Swedish e-Science Research Centre, and the Swedish National Graduate School for Neutron Scattering for funding. Computational resources were provided by the Swedish National Infrastructure for Computing.

- Kopp Lugli A, Yost CS, Kindler CH (2009) Anaesthetic mechanisms: Update on the challenge of unravelling the mystery of anaesthesia. *Eur J Anaesthesiol* 26:807–820.
- Franks NP (2006) Molecular targets underlying general anaesthesia. *Br J Pharmacol* 147:572–581.
- Forman SA, Miller KW (2011) Anesthetic sites and allosteric mechanisms of action on Cys-loop ligand-gated ion channels. *Can J Anaesth* 58:191–205.
- Burgos CF, Yévenes GE, Aguayo LG (2016) Structure and pharmacologic modulation of inhibitory glycine receptors. *Mol Pharmacol* 90:318–325.
- Garcia PS, Kolesky SE, Jenkins A (2010) General anesthetic actions on GABA(A) receptors. *Curr Neuropharmacol* 8:2–9.
- Forman SA, Chiara DC, Miller KW (2015) Anesthetics target interfacial transmembrane sites in nicotinic acetylcholine receptors. *Neuropharmacology* 96:169–177.
- Howard RJ, Trudell JR, Harris RA (2014) Seeking structural specificity: Direct modulation of pentameric ligand-gated ion channels by alcohols and general anesthetics. *Pharmacol Rev* 66:396–412.
- Zuo Y, et al. (2001) Dual action of n-alcohols on neuronal nicotinic acetylcholine receptors. *Mol Pharmacol* 60:700–711.
- Stevens R, Rüschi D, Solt K, Raines DE, Davies PA (2005) Modulation of human 5-hydroxytryptamine type 3A receptors by volatile anesthetics and n-alcohols. *J Pharmacol Exp Ther* 314:338–345.
- Miller PS, Aricescu AR (2014) Crystal structure of a human GABA<sub>A</sub> receptor. *Nature* 512:270–275.
- Zhu S, et al. (2018) Structure of the human synaptic GABA<sub>A</sub> receptor. *Nature* 559:67–72.
- Huang X, Chen H, Michelsen K, Schneider S, Shaffer PL (2015) Crystal structure of human glycine receptor- $\alpha$ 3 bound to antagonist strychnine. *Nature* 526:277–280.
- Du J, Lü W, Wu S, Cheng Y, Gouaux E (2015) Glycine receptor mechanism elucidated by electron cryo-microscopy. *Nature* 526:224–229.
- Morales-Perez CL, Noviello CM, Hibbs RE (2016) X-ray structure of the human  $\alpha$ 4 $\beta$ 2 nicotinic receptor. *Nature* 538:411–415.
- Hassaine G, et al. (2014) X-ray structure of the mouse serotonin 5-HT<sub>3</sub> receptor. *Nature* 512:276–281.
- Basak S, et al. (2018) Cryo-EM structure of 5-HT<sub>3A</sub> receptor in its resting conformation. *Nat Commun* 9:514.
- Nemecz Á, Prevost MS, Menny A, Corringer PJ (2016) Emerging molecular mechanisms of signal transduction in pentameric ligand-gated ion channels. *Neuron* 90:452–470.
- Prevost MS, et al. (2012) A locally closed conformation of a bacterial pentameric proton-gated ion channel. *Nat Struct Mol Biol* 19:642–649.
- Sauguet L, et al. (2014) Crystal structures of a pentameric ligand-gated ion channel provide a mechanism for activation. *Proc Natl Acad Sci USA* 111:966–971.
- Sauguet L, et al. (2013) Structural basis for ion permeation mechanism in pentameric ligand-gated ion channels. *EMBO J* 32:728–741.
- Basak S, Schmandt N, Gicheru Y, Chakrapani S (2017) Crystal structure and dynamics of a lipid-induced potential desensitized-state of a pentameric ligand-gated channel. *eLife* 6:e23886.
- Nury H, et al. (2011) X-ray structures of general anesthetics bound to a pentameric ligand-gated ion channel. *Nature* 469:428–431.
- Weng Y, Yang L, Corringer PJ, Sonner JM (2010) Anesthetic sensitivity of the *Gloeobacter violaceus* proton-gated ion channel. *Anesth Analg* 110:59–63.
- Fourati Z, et al. (2018) Structural basis for a bimodal allosteric mechanism of general anesthetic modulation in pentameric ligand-gated ion channels. *Cell Rep* 23:993–1004.
- Heusser SA, et al. (2013) Functional validation of virtual screening for novel agents with general anesthetic action at ligand-gated ion channels. *Mol Pharmacol* 84:670–678.
- Pace CN, Scholtz JM (1998) A helix propensity scale based on experimental studies of peptides and proteins. *Biophys J* 75:422–427.
- Sauguet L, et al. (2013) Structural basis for potentiation by alcohols and anesthetics in a ligand-gated ion channel. *Nat Commun* 4:1697.
- Spurny R, et al. (2013) Multisite binding of a general anesthetic to the prokaryotic pentameric *Erwinia chrysanthemi* ligand-gated ion channel (ELIC). *J Biol Chem* 288:8355–8364.
- Jayakar SS, Dailey WP, Eckenhoff RG, Cohen JB (2013) Identification of propofol binding sites in a nicotinic acetylcholine receptor with a photoreactive propofol analog. *J Biol Chem* 288:6178–6189.
- Johnson WD, 2nd, Howard RJ, Trudell JR, Harris RA (2012) The TM2 6' position of GABA(A) receptors mediates alcohol inhibition. *J Pharmacol Exp Ther* 340:445–456.
- LeBard DN, Hénin J, Eckenhoff RG, Klein ML, Brannigan G (2012) General anesthetics predicted to block the GLIC pore with micromolar affinity. *PLoS Comput Biol* 8:e1002532.
- Monod J, Wyman J, Changeux JP (1965) On the nature of allosteric transitions: A theoretical model. *J Mol Biol* 12:88–118.
- Ghosh B, Satyshur KA, Czajkowski C (2013) Propofol binding to the resting state of the *Gloeobacter violaceus* ligand-gated ion channel (GLIC) induces structural changes in the inter- and intrasubunit transmembrane domain (TMD) cavities. *J Biol Chem* 288:17420–17431.
- Young GT, Zwart R, Walker AS, Sher E, Millar NS (2008) Potentiation of  $\alpha$ 7 nicotinic acetylcholine receptors via an allosteric transmembrane site. *Proc Natl Acad Sci USA* 105:14686–14691.
- Jayakar SS, et al. (2014) Multiple propofol-binding sites in a  $\gamma$ -aminobutyric acid type A receptor (GABAAR) identified using a photoreactive propofol analog. *J Biol Chem* 289:27456–27468.
- Chiara DC, Dangott LJ, Eckenhoff RG, Cohen JB (2003) Identification of nicotinic acetylcholine receptor amino acids photolabeled by the volatile anesthetic halothane. *Biochemistry* 42:13457–13467.
- Lev B, et al. (2017) String method solution of the gating pathways for a pentameric ligand-gated ion channel. *Proc Natl Acad Sci USA* 114:E4158–E4167.
- Rienzo M, Lummis SC, Dougherty DA (2014) Structural requirements in the transmembrane domain of GLIC revealed by incorporation of noncanonical histidine analogs. *Chem Biol* 21:1700–1706.
- Rienzo M, Rocchi AR, Threatt SD, Dougherty DA, Lummis SC (2016) Perturbation of critical prolines in *Gloeobacter violaceus* ligand-gated ion channel (GLIC) supports conserved gating motions among Cys-loop receptors. *J Biol Chem* 291:6272–6280.
- England PM, Zhang Y, Dougherty DA, Lester HA (1999) Backbone mutations in transmembrane domains of a ligand-gated ion channel: Implications for the mechanism of gating. *Cell* 96:89–98.
- Purohit P, Auerbach A (2007) Acetylcholine receptor gating at extracellular transmembrane domain interface: The “pre-M1” linker. *J Gen Physiol* 130:559–568.
- Dang H, England PM, Farivar SS, Dougherty DA, Lester HA (2000) Probing the role of a conserved M1 proline residue in 5-hydroxytryptamine(3) receptor gating. *Mol Pharmacol* 57:1114–1122.
- Bouzat C, Bartos M, Corradi J, Sine SM (2008) The interface between extracellular and transmembrane domains of homomeric Cys-loop receptors governs open-channel lifetime and rate of desensitization. *J Neurosci* 28:7808–7819.
- Jaitheh M, Taly A, Hénin J (2016) Evolution of pentameric ligand-gated ion channels: Pro-loop receptors. *PLoS One* 11:e0151934.
- Murail S, Wallner B, Trudell JR, Bertaccini E, Lindahl E (2011) Microsecond simulations indicate that ethanol binds between subunits and could stabilize an open-state model of a glycine receptor. *Biophys J* 100:1642–1650.
- Tetko IV, et al. (2005) Virtual computational chemistry laboratory—Design and description. *J Comput Aided Mol Des* 19:453–463.
- Hansch C, Leo A, Hoekman D, eds (1995) *Exploring QSAR: Hydrophobic, Electronic, and Steric Constants* (Am Chem Soc, Washington, DC), Vol 2.
- Laurent B, et al. (2016) Sites of anesthetic inhibitory action on a cationic ligand-gated ion channel. *Structure* 24:595–605.
- Mowrey D, et al. (2013) Asymmetric ligand binding facilitates conformational transitions in pentameric ligand-gated ion channels. *J Am Chem Soc* 135:2172–2180.
- Olsen RW (2018) GABA<sub>A</sub> receptor: Positive and negative allosteric modulators. *Neuropharmacology* 136:10–22.
- Woll KA, et al. (2016) A novel bifunctional alkylphenol anesthetic allows characterization of  $\gamma$ -aminobutyric acid, type A (GABA<sub>A</sub>) receptor subunit binding selectivity in Synaptosomes. *J Biol Chem* 291:20473–20486.
- Hibbs RE, Gouaux E (2011) Principles of activation and permeation in an anion-selective Cys-loop receptor. *Nature* 474:54–60.
- Abraham MJ, et al. (2015) GROMACS: High performance molecular simulations through multi-level parallelism from laptops to supercomputers. *SoftwareX* 1–2:19–25.
- Humphrey W, Dalke A, Schulten K (1996) VMD: Visual molecular dynamics. *J Mol Graph* 14:33–38.
- Schmidtke P, Bidon-Chanal A, Luque FJ, Barril X (2011) MDpocket: Open-source cavity detection and characterization on molecular dynamics trajectories. *Bioinformatics* 27:3276–3285.
- Trott O, Olson AJ (2010) AutoDock Vina: Improving the speed and accuracy of docking with a new scoring function, efficient optimization, and multithreading. *J Comput Chem* 31:455–461.